Towards time domain finite element analysis of gravity gradient noise

Beker, M.G.; van den Brand, J.F.J.; Hennes, E.; Rabeling, D.S.

published in
Journal of Physics : Conference Series
2010

DOI (link to publisher)
10.1088/1742-6596/228/1/012034

document version
Publisher's PDF, also known as Version of record

Towards time domain finite element analysis of gravity gradient noise

2010 J. Phys.: Conf. Ser. 228 012034

(http://iopscience.iop.org/1742-6596/228/1/012034)

Journal of Physics: Conference Series **228** (2010) 012034 doi:10.1088/1742-6596/228/1/012034

Towards time domain finite element analysis of gravity gradient noise

M.G. Beker, J.F.J. van den Brand, E. Hennes, D.S. Rabeling

Nikhef, National Institute for Subatomic Physics, Science Park 105, 1098 XG Amsterdam, The Netherlands

E-mail: mbeker@nikhef.nl

Abstract. Gravity gradient noise generated by seismic displacements constitute a limiting factor for the sensitivity of ground based gravitational wave detectors at frequencies below 10 Hz. We present a finite element framework to calculate the soil response to various excitations. The accompanying gravity gradients as a result of the seismic displacement field can then be evaluated. The framework is first shown to accurately model seismic waves in homogenous media. Calculations of the gravity gradient noise are then shown to be in agreement with previous analytical results. Finally results of gravity gradient noise from a single pulse excitation of a homogenous medium are discussed.

1. Introduction

Advances in gravitational wave (GW) detection have, throughout the past 20 years, overcome many technical obstacles and suppressed a vast number of instrumental noise sources. At this moment first generation interferometric detectors have reached their design sensitivities and second generation detectors are poised to upgrade these sensitivities by a factor of 10 within the next decade [1] [2] [3]. Now research is starting to explore possibilities beyond the second generation detectors. A third generation of detectors will once again improve sensitivities by a factor of 10 over a broad frequency spectrum [4]. A particular challenge will be to detect signals at frequencies below 10 Hz. It is expected that sensitivity at these frequencies will be limited by fluctuations in the local gravitational field as a result of fluctuating density variations in the surrounding soil [5] [6] [7]. These field fluctuations couple directly to the interferometer test masses and are known as gravity gradient (or Newtonian) noise (GGN). A full understanding of seismic activity, seismic wave characteristics and how these affect GW detectors through gravity gradients is imperative to achieve the desired sensitivity. Sources of seismic noise include earthquakes, atmospheric and oceanic disturbances and cultural noise [8]. The latter is a result of human activity and infrastructure such as footsteps, traffic and machinery. Analytical descriptions of seismic activity fall short when considering a non-homogeneous medium or complex geologies. Here we present a time domain finite element (FE) framework to model seismic activity and discuss the impact of GGN on GW detectors.

2. Ambient ground motion and gravity gradient noise

As a result of seismic disturbances a displacement wave field is produced that is governed by the elasto-dynamic equations. The wave field in a homogeneous elastic medium can be expressed as

a combination of plane body waves [9]. Two types of body waves exist, pressure (P) and shear (S) waves [10]. In the case of P-waves the movement of a ground particles is parallel to the direction of wave propagation. For S-waves the particle motion is perpendicular to the direction of the wave. The characteristics of seismic waves can be described by the ground properties, parameterized by the Young's modulus, E, the density, ρ, and the Poisson ratio, ν, describing the relationship between shear and strain forces. The wave velocities are then given by

$$c_P = \sqrt{\frac{E(1-\nu)}{(1-2\nu)(1+\nu)\rho}}, \text{ and } \quad c_S = \sqrt{\frac{E}{2(1+\nu)\rho}}, \tag{1}$$

for P and S-waves respectively. Typical values for clay-like soils range from 500 - 1000 m/s for c_P, and 250 - 600 m/s for c_S. In a medium that is bounded by another medium, such as air, or is comprised of layers, surface and head waves also exist. Head waves emerge in stratified media where modes propagating along an interface, cause energy to radiate into the low velocity zone. Surface waves are typically referred to as Rayleigh and Love waves. Love waves involve particle motion parallel to the surface and transverse to the direction of propagation. They produce no density variations and therefore have no effect on gravity gradients [6]. Rayleigh waves are polarised perpendicular to the surface and vanish with depth. Solving the wave equation for harmonic Rayleigh waves results in the following displacement fields [11]

$$\begin{aligned} \xi_x &= iA(k_R e^{-\kappa_P z} - \zeta\kappa_S e^{-\kappa_S z})e^{i(k_R x-\omega t)}, \\ \xi_z &= -A(\kappa_P e^{-\kappa_P z} - \zeta k_R e^{-\kappa_S z})e^{i(k_R x-\omega t)}, \end{aligned} \tag{2}$$

where A is an arbitrary amplitude, t denotes time, ω denotes the angular frequency, z is the depth, k_R is the wave number of the Rayleigh wave, and $\kappa_S = \sqrt{k_R^2 - k_S^2}$ and $\kappa_P = \sqrt{k_R^2 - k_P^2}$ are decay factors related to the shear and pressure wave numbers. Finally, $\zeta = \sqrt{\kappa_P/\kappa_S}$. The horizontal Rayleigh wave speed, c_R, is slightly lower than the S-wave speed and when expressed in units of c_S is purely a function of ν. It can be found through $c_R/c_S = \chi$ where χ is the real root, in the range $0 < \chi < 1$ of the equation [11]

$$\chi^6 - 8\chi^4 + 8\left(\frac{2-\nu}{1-\nu}\right)\chi^2 - \frac{8}{1-\nu} = 0. \tag{3}$$

The above describes harmonic Rayleigh waves propagating far from the source. In reality, excitation of a medium results in a combination of all the different wave fields; body and surface.

As waves propagate through the medium, their amplitude decreases. This attenuation can be attributed to two factors; material and geometric damping. Geometrical damping is a result of energy spreading over an increasing area. The frequency dependent material damping involves energy lost due to friction. Seismic wave attenuation for homogeneous media, can be described by [12]

$$A_2 = A_1\left(\frac{r_1}{r_2}\right)^n e^{-\frac{\pi\eta f}{c}(r_2-r_1)}, \tag{4}$$

where A_1 and A_2 are the wave amplitudes at distance r_1 and r_2 from the source, n is the geometric damping coefficient, f is the frequency and c the propagation speed of the wave. The material damping is represented by the loss factor η. The geometric damping coefficient can be determined analytically by assessing the type of wave involved and the source type. For radial surface waves $n = 1/2$ while radial body waves within the medium decay with $n = 1$. For this paper η is set to zero.

For a given distribution of masses, which can be described by the mass density function $\rho(\mathbf{r}, t)$, the acceleration experienced by a test mass (i.e. an interferometer mirror) located at $\mathbf{y}$

can be written as

$$\mathbf{a}(\mathbf{y},t) = G\int_V \rho(\mathbf{r},t)\frac{\mathbf{r}'}{|\mathbf{r}'|^3}dV, \tag{5}$$

where $\mathbf{r}$ is the position of the mass volume dV and $\mathbf{r}' = \mathbf{r}-\mathbf{y}$. In our FE analysis the acceleration is the summation of the contributions from each node i with mass m_i located at $\mathbf{r}_i$. The acceleration at the test mass is given by

$$\mathbf{a} = \sum_i \mathbf{a}_i = \sum_i Gm_i\frac{\mathbf{r}'}{|\mathbf{r}'|^3}, \tag{6}$$

with G the universal gravitational constant. When a seismic disturbance is present, the nodes suffer a displacement denoted by $\xi_i(\mathbf{r},t)$. The gravity gradient acceleration due to these displacements is given by

$$\mathbf{a}^{NN}(\mathbf{y},t) = \sum_i(\nabla\otimes\mathbf{a}_i)^T\xi_i(\mathbf{r},t). \tag{7}$$

Note that in the gravity gradient calculations presented here, the mass associated with each node is assumed to be constant. The corresponding analytical expression can be obtained by substituting $m_i \to \rho dV$ and evaluating the resulting integral.

3. Finite element ground motion simulations

Simulation of the ground displacement fields was done with the FE software package *Comsol* [13]. In the FE framework we subdivide a 3D continuum into small hexahedral elements. Within each element the relevant physical parameters, like displacement and stress, are approximated by spline functions of arbitrary order. To confirm the ground motion response calculated by a FE model, comparison is made with analytical solutions described in the previous paragraph.

The FE displacement wave fields for one wavelength of a Rayleigh wave propagating in the x direction have been plotted in Fig. 1. It is interesting to note the sign change in the particle movement in the x direction. This occurs at a depth of about $0.2\lambda_R$. In Fig. 1b the maximum amplitude in both the x and z displacements are plotted, the two are separated by a phase difference of $\pi/2$. These are in good agreement with the analytical solutions of Eq. (2).

A homogenous half-space was simulated by creating a half-sphere model with no reflection of waves incident to the spherical boundary. In view of symmetry the model could be further simplified to a quarter half-space with symmetric boundary conditions on the vertical surfaces. A single vertical excitation force was applied uniformly within a circular area at the origin with a time dependent factor given by $F(t) = A\sin^2(\pi t/T_e)$ for $0 \le t \le T_e$ where T_e is the excitation period. The amplitude scaling factor, A, was adjusted to create a vertical displacement at the excitation point of 1 μm. The model has parameters $E = 10$ GPa, $\rho = 2.0$ g/cm^3, $\nu = 0.25$ and a radius of 2.2 km. This results in wave speeds of $c_P = 800$ m/s, $c_S = 462$ m/s and $c_R = 420$ m/s. To check the consistency of the model with analytical expectations the arrival times and geometric damping of the wave fields can be studied. No material damping was implemented in this model. Fig. 2a shows the FE results of seismic displacements along with expected arrival times at a location on the surface and at a depth of 800 m. Note the phase difference of $\pi/2$ between the x and z displacements of the Rayleigh wave. The rms wave amplitude with increasing distance from the source across the surface and within the medium are plotted in Fig. 2b. As expected from Eq. (4) the wave attenuation is proportional to $1/\sqrt{r}$ along the surface and $1/r$ within the medium.

4. Comparison with previous analytical GGN results

The calculation of GGN via FE models was validated by creating simple rectangular homogenous half-space models, equivalent to those discussed by Saulson for a surface detector [5]. The

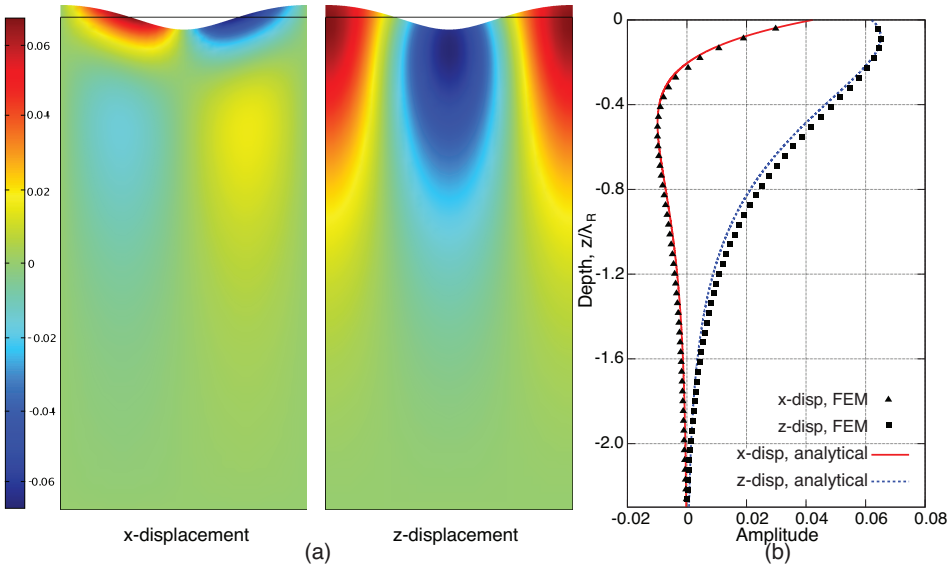

Figure 1. (a) Rayleigh wave displacement fields for a wave propagating in the x direction. (b) FE and analytical calculations of Rayleigh wave displacements. The x and z components attenuate differently with depth. The x component changes sign at a depth of about 0.2 λ_R.

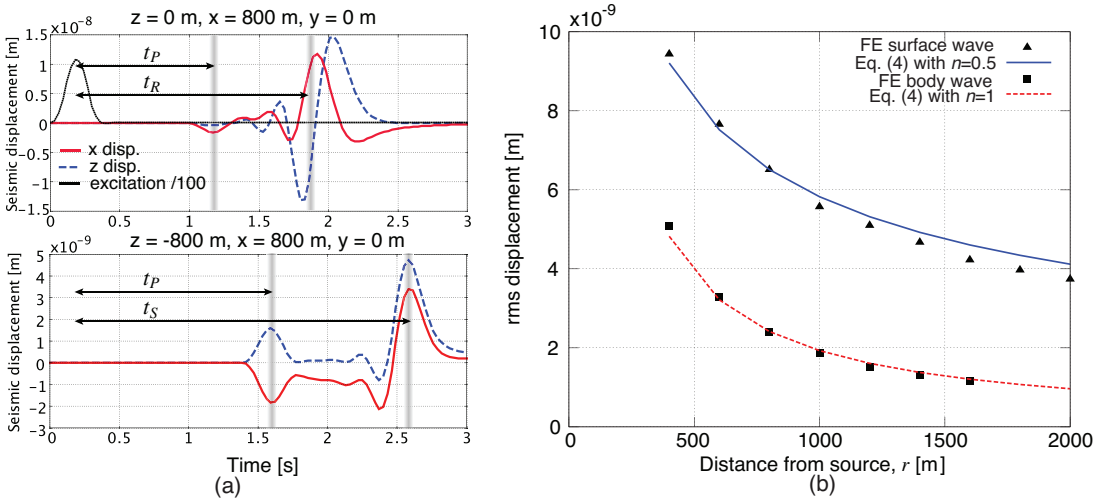

Figure 2. (a) FE ground displacement measurements at a surface and subterranean location after a pulse excitation. P, S and Rayleigh wave arrival times are indicated. (b) The FE results for the rms amplitude of the surface and body waves with increasing distance from the source. The geometric damping contribution to Eq. (4) is plotted for comparison.

isotropic, elastic half-space with $\rho = 1.8$ g/cm^3, $\nu = 0.33$, $c_P = 440$ m/s and $c_S = 220$ m/s was excited on one boundary to yield plane harmonic pressure waves scaled to a flat ambient seismic noise spectrum of 1 nm/$\sqrt{\text{Hz}}$ between 1 and 10 Hz and the subsequent nodal displacements were recorded as a function of time. Boundary conditions were set such that no reflections occurred and seismic waves were continuous. With this input spectrum the gravity gradient displacement noise amplitude at the interferometer output was calculated and the result is shown in Fig. 3b. The FE results are compared with the analytic results of Saulson and Hughes and Thorne [5][6].

To facilitate comparison, an integral cut-off radius equal to that used in Saulson's analysis ($r_{\text{cutoff}} = \lambda/4$) was employed in the summation process. Fig. 3 shows that good agreement is obtained. To assess the effect of this cut-off the above model was calculated analytically with Eq. (5). Removing the cut-off leads to an increase of GGN by about a factor 2 (see Fig. 3). The FE results approach those of the analytic expression in the limit that r_{cutoff} decreases to zero.

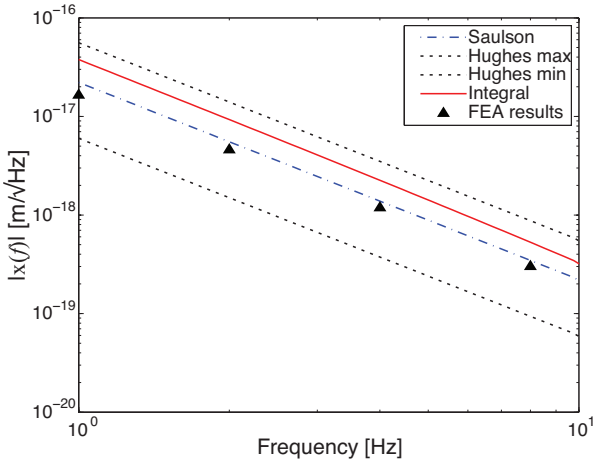

Figure 3. FE calculation of the Newtonian displacement noise amplitude for a surface detector. For comparison the results of Saulson, Hughes and Thorne, and the analytic integral are shown.

5. GGN results from pulse excitations on a homogeneous medium

The pulse excitations and the half-sphere model described in section 3, were used to investigate FE gravity gradient modeling (see Fig. 4). The nodal displacements were recorded as a function of time and the GGN was calculated at various depths on a vertical line at a distance $\lambda_P = 800$ m from the z-axis. In order to artificially separate the contributions of the surface and body waves to the GGN acceleration the nodes with a depth less than 200 m were summed separately to those deeper that 200 m. The respective surface and body contributions were combined to give a total acceleration. Note that for times shortly after the excitation, this distinction is not precise. The results for a test mass at the surface and a test mass at a depth of λ_P are shown in Fig. 4. Only the GGN acceleration in the horizontal direction is shown since it has the largest effect on the performance of an interferometer. The expected arrival times of the different waves are indicated in the figures and show that the Rayleigh wave dominates the GGN contribution of a detector on the surface. At a depth of λ_P the arrival of the S and P-waves can clearly be distinguished, the S-wave producing a larger contribution, attributed to the larger seismic displacements seen in Fig. 2a. The GGN contribution of a wave is initially negative as the wave approaches then changes sign as the wave passes by the test mass. It is interesting to note that the sign change of the surface contributions between a surface and underground detector. This is due to the sign change of the horizontal component of the Rayleigh wave for depths larger than $0.2\lambda_R \approx 80$ m. The figure also shows that GGN builds up before any seismic disturbance actually reaches the test mass and for short times is only dependent on surface contributions.

6. Conclusions

A time domain finite element framework has been presented that successfully models seismic motion. The displacement fields of a Rayleigh wave are accurately modelled. By investigating pulse excitations of a homogenous half-space it is shown that all wave types are excited. These propagate from the source as predicted by theoretical models and adhere to the geometrical damping laws. Gravity gradient accelerations from a homogeneous half-space are calculated and show agreement with previous analytical results. Finally results are presented

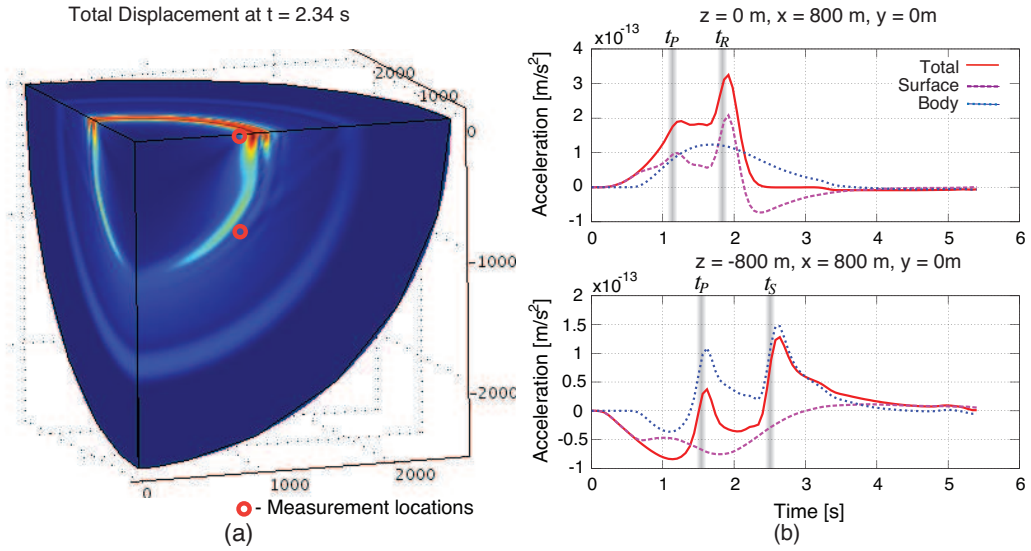

Figure 4. (a) Total displacement for a time domain simulation at 2.34 seconds after a 1 μm pulse excitation at the center of the half-sphere. (b) Time domain evolution of GGN acceleration at a surface (z=0 m) and underground (z=-800 m) test mass. Only the horizontal component of the GGN acceleration is shown. Arrival times of Rayleigh, S and P-waves are also indicated.

of GGN accelerations for the pulse excitation on a homogeneous half-sphere. This analysis indicates strong contributions from Rayleigh waves for a surface detector and body waves for a subterranean detector. This paper has shown that a FE framework can be an effective tool in investigating gravity gradients for future, possibly subterranean, gravitational wave detectors. This allows further research into quantitive effects of seismic motion on GGN and implications of geology and infrastructure.

Acknowledgments

This work has been performed with the support of the European Commission under the Framework Programme 7 (FP7) Capacities, project Einstein Telescope design study (Grant Agreement 211743), http://www.et-gw.eu/. This work is part of the research programme of the Foundation for Fundamental Research on Matter (FOM), which is financially supported by the Netherlands Organisation for Scientific Research (NWO).

References

[1] Acernese F *et al.* 2008 *Class. Quantum Grav.* **25** 184001
[2] Sutton P 2008 *J. Phys.: Conf. Ser.* **110** 062024
[3] Danzmann K 1995 *Proc. First E. Amaldi Conf. Grav. Wave Exp. (Rome)*
[4] Hild S *et al.* A 2008 Pushing towards the ET sensitivity using 'conventional' technology `arXiv.org:0810.0604`
[5] Saulson P 1984 *Phys. Rev. D* **30** 732–736
[6] Hughes S and Thorne K 1998 *Phys. Rev. D* **58** 122002
[7] Beccaria M *et al.* 1998 *Class. Quantum Grav.* **15** 3339–3362
[8] Peterson J 1993 *U.S. Department of Interior Geological Survey* Open-File Report 93-322
[9] Schevenels M 2007 Ph.D. thesis Katholieke Universiteit Leuven
[10] Achenbach J 1973 *Wave Propagation in Elastic Solids* (Amsterdam: North-Holland) pp 187–194
[11] Hassan W and Nagy P B 1998 *J. Acoust. Soc. Am.* **104** 3107
[12] Kim D S and Lee J S 2000 *Soil Dyn. and Earthq. Eng.* **19** 115–126
[13] Comsol Multiphysics version 3.5a URL `www.comsol.com`